

Solar Photovoltaic Assessment with Large Language Model

Muhao Guo, Yang Weng^a

^a*Department of Electrical, Computer and Energy Engineering, Arizona State University, Goldwater Center for Science and Engineering, 650 E Tyler Mall, Tempe, 85281, AZ, USA*

Abstract

Accurate detection and localization of solar photovoltaic (PV) panels in satellite imagery is essential for optimizing microgrids and active distribution networks (ADNs), which are critical components of renewable energy systems. Existing methods lack transparency regarding their underlying algorithms or training datasets, rely on large, high-quality PV training data, and struggle to generalize to new geographic regions or varied environmental conditions without extensive re-training. These limitations lead to inconsistent detection outcomes, hindering large-scale deployment and data-driven grid optimization. In this paper, we investigate how large language models (LLMs) can be leveraged to overcome these challenges. Despite their promise, LLMs face several challenges in solar panel detection, including difficulties with multi-step logical processes, inconsistent output formatting, frequent misclassification of visually similar objects (e.g., shadows, parking lots), and low accuracy in complex tasks such as spatial localization and quantification. To overcome these issues, we propose the PV Assessment with LLMs (PVAL) framework, which incorporates task decomposition for more efficient workflows, output standardization for consistent and scalable formatting, few-shot prompting to enhance classification accuracy, and fine-tuning using curated PV datasets with detailed annotations. PVAL ensures transparency, scalability, and adaptability across heterogeneous datasets while minimizing computational overhead. By combining open-source accessibility with robust methodologies, PVAL establishes an automated and reproducible pipeline for solar panel detection, paving the way for large-scale renewable energy integration and optimized grid management.

Keywords: Solar Photovoltaics, Solar Panel Detection, Satellite Imagery,

1. Introduction

The global transition toward renewable energy has significantly influenced the operation and planning of power systems, particularly in active distribution networks (ADNs) and microgrids [1]. As a leading source of clean energy, solar photovoltaic (PV) technology has become increasingly important for decentralizing power generation and enhancing grid resilience [2]. To realize these benefits, accurate detection and mapping of solar PV installations in satellite imagery are critical for efficient energy management, demand-response optimization, and the seamless integration of distributed energy resources (DERs) [3]. However, the widespread adoption of solar panels has led to an exponential increase in the amount of imagery data, necessitating highly scalable and adaptable approaches for PV identification.

Early approaches to solar panel detection from imagery relied on traditional machine learning models, such as Logistic Regression [4], Random Forest [5], and Support Vector Machines based methods [6], often employing handcrafted features like texture and color.

Although these methods were relatively efficient and required fewer training samples, they lacked the capacity to generalize to diverse spatial patterns. More recent research has turned towards deep learning [7, 8], particularly Convolutional Neural Network (CNN)-based models [9], which have demonstrated superior performance in extracting vision features from imagery data. Notable efforts such as Deep Solar [10] showcased large-scale solar panel mapping using Inception-v3, while U-Net [11] enabled global solar mapping. However, these methods often require substantial annotated datasets [12, 13], intensive computational resources, and frequent retraining to adapt to changing conditions in different geographical regions and environmental contexts.

These limitations highlight a pressing need for flexible, transparent, and resource-efficient solutions. Large language models (LLMs) have emerged as a promising paradigm for detection tasks with limited labels [14], owing to their extensive pre-training on diverse data sources. Although originally developed for natural language processing (NLP), advanced LLMs such as OpenAI’s GPT series [15], Google’s PaLM [16], and Meta’s LLaMA [17] have extended their capabilities to multimodal tasks, including image analysis. LLMs can capture rich contextual information [18, 19, 20] and handle het-

erogeneous inputs and varying contexts, making them particularly suitable for the dynamic environments typical of ADNs and microgrids [21].

Although LLMs show great promise for solar panel detection, they face significant challenges. Firstly, LLMs often struggle with multi-step logical processes essential for accurately identifying and assessing solar panels [22]. This difficulty arises because solar panel detection typically requires sequential reasoning, such as distinguishing panels from similar structures, understanding spatial relationships, and integrating contextual information from satellite imagery. Additionally, LLMs can exhibit inconsistencies in output formatting [23]. This inconsistency can lead to increased manual intervention, reducing the overall efficiency and scalability of solar energy management workflows.

Another major challenge is the misclassification of visually similar objects. For example, shadows, parking lots, or other flat surfaces may be incorrectly identified as solar panels due to their comparable appearance in satellite images. This issue is exacerbated in environments with high visual complexity or varying lighting conditions, which can obscure or distort the features LLMs rely on for accurate classification. Furthermore, LLMs often display low accuracy in complex tasks such as spatial localization and quantification of solar panels. Accurate spatial localization requires precise mapping of panel locations, while quantification involves estimating the number and capacity of panels, both of which demand high precision and reliability.

To address the challenges associated with LLMs in solar panel detection, we propose prompting and fine-tuning strategies. First, solar panel detection involves analyzing complex rooftop images to accurately identify and assess solar installations. To manage this complexity, we implement task decomposition within our PVAL framework. We begin by defining the overall objective in the prompt, guiding the model to understand the context and goals of the analysis. The task is then broken down into specific steps: first, the model performs a holistic image analysis to detect potential solar panels; second, it pinpoints the exact locations of these panels within predefined regions; and third, it estimates the quantity of panels based on their arrangement and visibility. This structured approach ensures that each sub-task is handled systematically, reducing the likelihood of errors and improving the overall accuracy of detection. By decomposing the task, we enable the LLM to focus on manageable components, thereby enhancing its ability to process complex visual data effectively.

Second, consistent and interpretable outputs are crucial for integrating

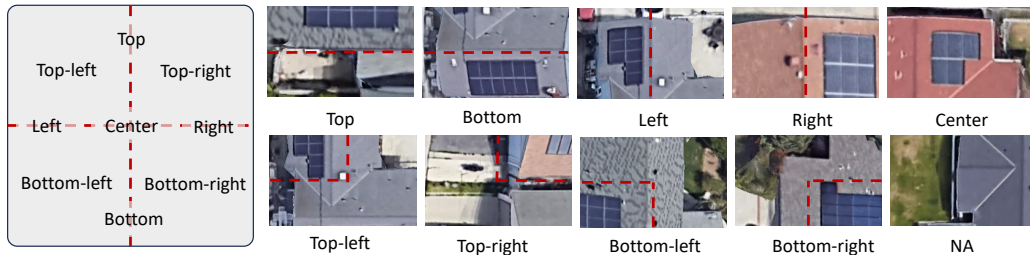


Figure 1: Illustration of all possible solar panel locations as defined in the work, accompanied by representative image examples for each category. The locations include *Top*, *Bottom*, *Left*, *Right*, *Center*, *Top-left*, *Top-right*, *Bottom-left*, *Bottom-right*, and “NA” (indicating no solar panels).

detection results into existing solar energy management systems. To achieve this, we employ output standardization by defining a JSON-based response format. This standardized structure includes key fields such as “*solar panels present*”, “*location*”, and “*quantity*”, each with predefined possible values to ensure uniformity. For example, the “*location*” field uses a detailed classification schema that divides the image into specific regions like “*top-left*” or “*center*” as illustrated in our visual schema (Figure 1). This standardization addresses the problem of inconsistent output formats, facilitating seamless data integration into geographic information systems (GIS) and energy management platforms. By ensuring that all outputs adhere to a uniform format, we eliminate the need for additional preprocessing, thereby streamlining workflows and enhancing the scalability of our detection system.

Third, accurate classification of solar panels, especially when distinguishing them from visually similar objects like shadows or parking lots, is a significant challenge. To address this issue, we utilize few-shot prompting by incorporating a limited number of highly relevant examples within the prompt. These examples include both positive cases (where solar panels are present) and negative cases (where they are absent), providing the LLM with clear references on how to handle different scenarios. For instance, one example might specify the detection of solar panels in the “*top-left*” quadrant with a quantity range of “*0 to 1*”, while another example indicates no panels detected by marking “*location*” and “*quantity*” as “*NA*”. By using five-shot prompting, we enhance the model’s ability to generalize from these examples, improving its classification accuracy without the need for extensive labeled datasets. This approach mitigates misclassification issues, enabling the LLM

to better distinguish between similar-looking objects and thereby increasing the reliability of solar panel detection.

Last, another challenge for LLMs in solar panel detection is handling complex spatial localization and quantification tasks. Accurate spatial localization requires precise mapping of panel locations, while quantification involves estimating the number and capacity of panels, both of which demand high precision and reliability. To overcome these limitations, we investigate fine-tuning strategies within our PVAL framework that complement the prompting techniques. By fine-tuning the LLM on specialized datasets that include annotated satellite images with detailed spatial information, the model can better understand and perform multi-step reasoning required for localization and quantification.

An additional benefit of PVAL is its capacity to provide nuanced likelihood and confidence values for identified solar panels. While conventional computer vision techniques have explored confidence scoring [24], LLMs can produce richer, context-aware assessments [25]. These confidence and likelihood metrics enable auto-labeling of large-scale datasets, reducing the need for manual annotation and enhancing system scalability. Consequently, powergrid operators can efficiently manage extensive data, ensuring accurate and reliable integration into ADNs and microgrids.

In this work, we explore solar panel detection by proposing PVAL that combines large language models (LLMs) with data engineering, prompt engineering, and fine-tuning strategies. The key contributions of this paper are:

1. **Prompting Strategies for PV Detection:** We address challenges such as misclassification and inconsistent outputs by implementing a combination of task decomposition, standardized output formatting, and few-shot prompting. These strategies enhance the interpretability of results and optimize the model’s ability to understand spatial and numerical information in satellite imagery, thereby improving detection accuracy and reliability.
2. **Robust Fine-tuning Techniques:** To mitigate geographic and environmental variability, we employ robust fine-tuning methods within our PVAL framework. By fine-tuning the LLM on specialized, curated datasets that include annotated satellite images with detailed spatial information, we ensure consistent performance across diverse regions and varying imaging conditions.

3. **Scalable and Adaptable Framework:** PVAL scales seamlessly across diverse U.S. regions, achieving high accuracy not only in detecting solar panels but also in localizing and quantifying them. This adaptability ensures robust performance in varied spatial and regional contexts, making it ideal for large-scale applications.
4. **Confidence-Driven Auto-Labeling Mechanism:** We introduce an auto-labeling mechanism driven by confidence and likelihood metrics. This mechanism enables the automatic labeling of large-scale datasets, significantly reducing the need for manual annotation. Consequently, powergrid operators can efficiently manage extensive data, ensuring accurate and reliable integration into Advanced Distribution Networks (ADNs) and microgrids.

Harnessing LLMs’ multimodal capabilities to detect solar panels and bridging prompt engineering and fine-tuning techniques, this research lays the groundwork for more intelligent, adaptive, and scalable solutions. We aim to facilitate the sustainable transformation of distribution networks and microgrids, supporting broader integration of renewable energy sources and paving the way towards smarter, more resilient power systems.

2. Problem Description

The widespread adoption of photovoltaic (PV) systems necessitates scalable, accurate, and efficient methodologies for their detection, localization, and quantification using satellite imagery. Current detection approaches encounter challenges due to the vast spatial heterogeneity in rooftop structures, varying environmental conditions, and the inherent limitations of traditional detection systems. Traditional convolutional neural network (CNN)-based models, while effective in feature extraction, require extensive annotated datasets and frequent retraining to adapt to different geographical regions and environmental contexts. Moreover, these models often struggle with the misclassification of visually similar objects—such as shadows, parking lots, and flat surfaces—which leads to reduced accuracy and increased manual intervention.

Formally, let the input satellite image be represented as I . The objective is to develop a function $f(I)$ that maps the input image to a set of outputs $\{D, L, Q, C\}$, where D indicates the binary detection of the presence of solar panels, L specifies the spatial localization of panels within the image I , Q

represents the quantification of the number of solar panels in the image, and C provides a credibility score representing the likelihood of correct detection, where $C \in [0, 1]$. The solution must ensure robust performance across diverse geographical regions, rooftop configurations, and varying environmental conditions. Additionally, the outputs $\{D, L, Q, C\}$ must be interpretable and seamlessly integrable into decision-making frameworks for active distribution networks (ADNs) and microgrids.

This work investigates how to leverage LLMs to process satellite imagery for PV detection. By incorporating data engineering, prompt engineering, and fine-tuning, the proposed PVAL efficiently detects, localizes, and quantifies solar panels while generating structured outputs with confidence metrics. PVAL emphasizes scalability, adaptability, and minimal reliance on manual annotations, providing a transformative solution for grid planning, renewable energy integration, and operational optimization.

3. Methodology

This section describes how PVAL can leverage LLMs for solar panel detection. PVAL incorporates data engineering, prompt engineering strategies, fine-tuning, and a dual-metric auto-labeling mechanism. Figure 2 illustrates the complete workflow of our approach.

3.1. Data Engineering

Data engineering is a foundational component of PVAL ensuring that the model is trained and evaluated on high-quality, well-structured datasets. PVAL incorporates three stages: data collection, image slicing, and labeling.

3.1.1. Data Collection

The process begins by identifying geographic coordinates of solar panel installations from OpenStreetMap (OSM) via the Overpass API. These coordinates guide the retrieval of high-resolution satellite imagery using the Google Maps Static API. To ensure representativeness, we target diverse U.S. regions: Seattle, WA; Orlando, FL; Osage Beach, MO; Harlem, NY; Tempe, AZ; and Santa Ana, CA. Capturing a wide array of climatic conditions, urban densities, and architectural styles enhances the model’s ability to generalize across heterogeneous environments (see Figure 3).

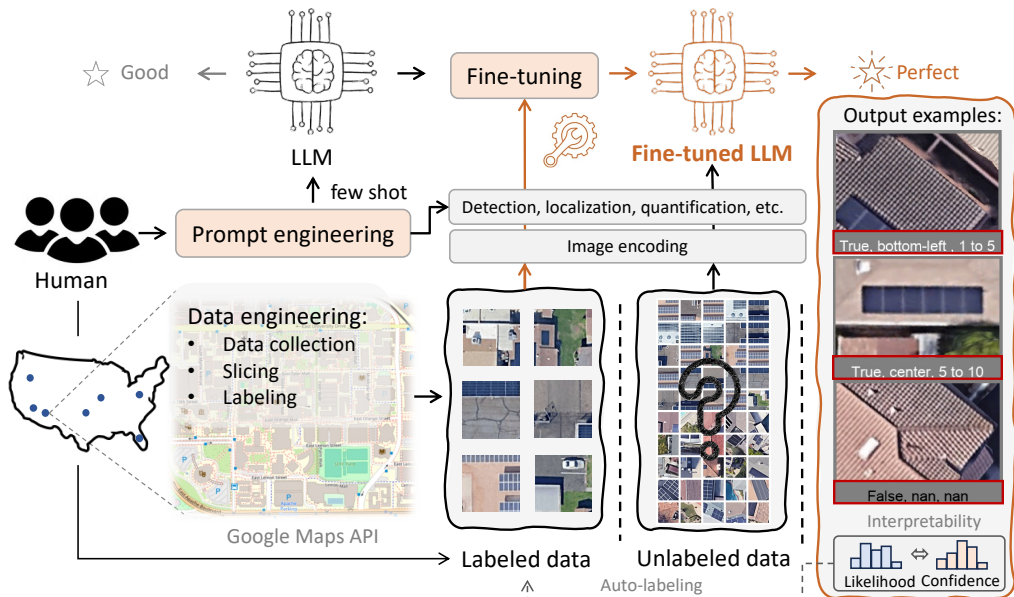


Figure 2: Workflow for solar panel detection, localization, and counting using LLMs. The framework combines data engineering, prompt engineering, and fine-tuning to improve accuracy, with outputs including predictions with likelihood and confidence values.

3.1.2. Image Slicing

To enhance detection granularity and scalability, we divide each high-resolution satellite image into a 4×4 grid, resulting in 16 equally sized tiles. The systematic slicing increases the number of training examples while preserving image resolution. Smaller solar panels remain distinguishable, enabling the model to identify, localize, and count panels at a finer spatial scale.

3.1.3. Data Labeling

We employ manual annotation to label each tiled image, recording the presence, location, and estimated quantity of solar panels. The human-in-the-loop approach ensures high-quality ground truth labels, facilitating effective fine-tuning and reliable performance evaluations [26].

3.2. Model Architecture and Input Encoding

The proposed PVAL system leverages the capabilities of GPT-4o, a large multimodal model built upon the transformer architecture, renowned for its ability to process and reason over both textual and visual inputs through

integrated attention mechanisms [27]. This section outlines the core model components and how satellite imagery is encoded for solar panel detection.

GPT-4o extends traditional transformer architectures by incorporating a vision encoder that transforms raw images into high-level embeddings. These visual embeddings are then integrated with language tokens, enabling unified multimodal reasoning. Unlike conventional vision transformers that apply self-attention directly to patches of image data, GPT-4o relies on a pretrained image encoder to process satellite imagery, followed by transformer layers that jointly reason over visual and textual information.

For the text modality, the core transformer uses self-attention mechanisms, formulated as:

$$\text{Attention}(Q, K, V) = \text{Softmax}\left(\frac{QK^T}{\sqrt{d_k}}\right)V, \quad (1)$$

with query, key, and value matrices Q, K, V derived from token embeddings. Multi-head attention extends this formulation as:

$$\text{MHA}(Q, K, V) = \text{Concat}(\text{head}_1, \dots, \text{head}_h)W^O, \quad (2)$$

allowing the model to attend to different subspaces in parallel.

Position-wise feed-forward networks (FFNs) and residual connections, combined with layer normalization, enhance non-linear representation capacity:

$$\text{FFN}(x) = \text{ReLU}(xW_1 + b_1)W_2 + b_2. \quad (3)$$

For input processing, satellite images are uploaded and internally encoded by GPT-4o’s vision subsystem. Although the raw image data is transmitted using formats such as *base64 encoding* [28], the model does not process base64 strings directly. Instead, images are converted into embeddings that the model can use in conjunction with textual prompts.

The prompts are carefully structured to guide the model’s attention toward image understanding tasks such as detecting, localizing, and quantifying solar panels. Outputs are returned as structured JSON, capturing information such as panel presence, approximate count, and bounding box location. This format facilitates integration with renewable energy monitoring platforms.

By combining prompt engineering with multimodal attention, PVAL enables GPT-4o to generalize across varied environmental and geographic conditions, achieving reliable solar panel detection from satellite imagery.

3.3. Prompting Strategies for PV Detection

Accuracy, scalability, minimizing ambiguity, and interpretability are critical requirements for applying LLMs to solar panel detection in satellite imagery. Accuracy ensures precise identification and classification of solar panels, while scalability allows the approach to handle large and diverse datasets efficiently. Minimizing ambiguity in outputs is crucial for reliable interpretation, and interpretability ensures that the generated results align seamlessly with downstream applications such as geospatial mapping and performance evaluation.

We address these requirements through prompt engineering strategies incorporating task decomposition [29], output standardization [30], and few-shot prompting [31]. Task decomposition allows the model to break down complex tasks into manageable sub-tasks, guiding the LLM to systematically identify solar panel presence, location, and quantity. Output standardization ensures consistent and interpretable results through a predefined JSON structure, minimizing variability and ambiguity in the outputs. Few-shot prompting enhances the model’s adaptability by providing illustrative examples, allowing it to generalize across diverse scenarios without extensive retraining.

3.3.1. Task Decomposition

```
Prompt – Task Decomposition

Identify the presence of solar panels in images of residential rooftops, and determine their locations and quantity within the images. You will be provided with images that may contain residential rooftop solar systems. Analyze each image to detect solar panels.

Steps:

1. Image Analysis : Examine the entire image to identify any objects that appear to be solar panels.
2. Panel Location : Determine the coordinates or area within the image where the solar panels are located.
3. Panel Quantification : Calculate or estimate the number of solar panels based on their appearance and arrangement.
```

The prompt begins with a clear task description, outlining the objective of analyzing rooftop images to detect solar panels, as shown in the Prompt box 3.3.1. The description ensures the model understands the task’s overall goal and context. The process is detailed through steps that guide the model to examine image holistically, identify solar panel locations using predefined regions, and estimate the PV quantity based on arrangement and visibil-

ity. The progression breaks the task into manageable sub-tasks, enabling a structured approach.

3.3.2. Output Standardization

```
Prompt – Output Standardization

The output should be in JSON format, structured as follows, with each field restricted to specific possible values for consistency and accuracy:

"solar_panels_present": A boolean value indicating if solar panels are detected.
Possible values: [true, false]

"location": A description or coordinates indicating where the panels are located within the image. Possible values: [left, right, bottom, top, top-left, top-right, bottom-right, bottom-left, center, NA]

"quantity": The number of solar panels detected in the image. Possible values: [0 to 1, 1 to 5, 5 to 10, 10 to inf, NA]

"likelihood_of_solar_panels_present": A value indicating the probability of solar panels being present. Possible values: A decimal range from 0.00 to 1.00

"confidence_of_solar_panels_present": A value indicating the model's confidence in its prediction. Possible values: A decimal range from 0.00 to 1.00
```

To ensure consistent and interpretable outputs, we define a standardized JSON-based response format. The JSON structure is shown in Prompt box 3.3.2 including essential fields such as “*solar panels present*”, which indicates whether solar panels are detected; “*location*”, which specifies the spatial region or quadrant where the panels are located; and “*quantity*”, which estimates the number of panels. In addition, fields of “*likelihood of solar panels present*” and “*confidence of solar panels present*” provide quantitative measures of the reliability of the predictions, enhancing interpretability and enabling users to assess the strength and uncertainty of the outputs [32].

The design of the “*location*” field incorporates a detailed classification schema for spatial localization, dividing the image into regions such as “*Top*”, “*Bottom*”, “*Left*”, “*Right*”, “*Center*”, and quadrants like “*Top-left*” and “*Bottom-right*”, etc. The spatial schema is illustrated in Figure 1, which provides a visual representation of all possible locations with example images for each category. These examples showcase common rooftop configurations where solar panels may be present or absent, such as panels centralized on a roof or distributed across specific quadrants. For cases where no solar panels are detected, the “*location*” field is assigned the value “*NA*”, ensuring completeness and consistency in the output.

The PVAL classification schema plays a critical role in the design of the

prompt, as it enables the LLM to focus on specific spatial patterns and ensures that the predictions are both interpretable and actionable. By dividing the image into discrete regions and associating these regions with representative examples, the model gains a structured understanding of spatial relationships. Dividing the image not only improves the clarity of the outputs but also enhances the model’s ability to generalize across diverse rooftop configurations and environmental conditions. The structured prompt, coupled with the spatial schema, establishes a clear connection between the input imagery and the model’s output, ensuring that the predictions align with real-world scenarios. In addition, we set the “temperature” parameter for LLM to zero to ensure consistency.

3.3.3. Few-shot Prompting

```
Prompt – Few-shot
# Example 1 (Solar) :
{ "solar_panels_present" : true,
  "location" : "top-left",
  "quantity" : "0 to 1",
  "likelihood_of_solar_panels_present" : 0.98,
  "confidence_of_solar_panels_present" : 0.90 }
# Example 2 (No Solar) :
{ "solar_panels_present" : false,
  "location" : "NA",
  "quantity" : "NA",
  "likelihood_of_solar_panels_present" : 0.21,
  "confidence_of_solar_panels_present" : 0.87 }
```

To improve generalization and adaptability, we integrate few-shot examples within the prompt. As shown in Prompt box 3.3.3, these examples demonstrate both positive and negative cases, helping the model generalize across a variety of scenarios. For instance, one example shows the case of solar panels being detected, with their location specified as the “*top-left*” and their quantity as a range, such as “*0 to 1*”. Another example illustrates the absence of solar panels, with fields like “*location*” and “*quantity*” marked as “*NA*”. These examples serve as a reference for the LLM, clarifying how to handle different inputs and cases. In practice, we use five-shot prompting.

The prompt engineering strategies in this work establish a scalable framework for applying LLMs to complex geospatial tasks. By integrating task decomposition, output standardization, and few-shot prompting, PVAL aligns

LLM capabilities with the demands of large-scale solar panel detection.

3.4. Robust Fine-Tuning Techniques

Adapting LLMs to specialized tasks like solar panel detection in satellite imagery requires domain-specific fine-tuning [33]. Although LLM excels at general-purpose understanding, it has to be refined to interpret complex rooftops, diverse imaging conditions, and varied environmental factors.

We employed OpenAI’s API infrastructure for the fine-tuning process, preparing the dataset in JSON Lines (JSONL) format. Each entry contained base64-encoded images, the proposed prompts, and ground truth labels, ensuring a consistent and reproducible pipeline. For the classification task, the supervised fine-tuning procedure optimized model parameters via cross-entropy loss, penalizing misclassifications and reinforcing accurate predictions:

$$\mathcal{L} = -\frac{1}{N} \sum_{i=1}^N [y_i \log(\hat{y}_i) + (1 - y_i) \log(1 - \hat{y}_i)], \quad (4)$$

where N is the total number of samples, y_i represents the ground truth label for the i -th sample, \hat{y}_i denotes the predicted probability of the positive class for the i -th sample. The cloud-based workflow is efficiently scaled to large, heterogeneous datasets, making it easily adaptable to other geospatial analysis tasks. By bridging the gap between general LLM capabilities and specific geospatial requirements, the fine-tuned GPT-4o model underscores the promise of LLMs in large-scale solar panel detection and energy resource planning.

3.5. Likelihood and Confidence Mechanism for Auto-Labeling

PVAL harnesses both likelihood and confidence metrics to automatically label large-scale datasets, that can potentially be utilized for semi-supervised learning, thereby reducing manual annotation overhead.

Likelihood quantifies the probability that solar panels are present in the imagery. Higher likelihood values indicate stronger evidence supporting the presence of solar panels. Specifically, values approaching 1 suggest a strong match to features characteristic of solar panels, implying a high probability of their presence. Conversely, values closer to 0 denote a weak or negligible match, suggesting their absence.

Confidence reflects the language model’s internal certainty regarding its identification. Confidence values near 1 signify that the model is highly

assured in its prediction, while values closer to 0 indicate greater uncertainty about the decision.

Likelihood and confidence metrics provide complementary insights for the auto-labeling process. In a true positive case, high likelihood combined with high confidence indicates that the model both detects solar panels accurately and does so with strong conviction, reinforcing the reliability of the automatic label. In contrast, a false negative with low confidence may highlight challenging conditions—such as complex rooftop geometries or poor image quality—thereby prompting operators to verify the label through additional data or manual inspection.

By employing this dual-metric approach in the auto-labeling mechanism, power grid operators can manage extensive datasets, ensuring accurate and reliable information integration into ADNs and microgrids. High-confidence predictions can be utilized for automated labeling, streamlining the process of annotating data for future model training. In contrast, low-confidence predictions can be flagged for manual review, enabling further data collection or targeted model refinement to enhance overall system performance. This flexible, transparent framework empowers stakeholders to make data-driven decisions in monitoring and managing distributed renewable energy resources.

4. Simulation and Analysis

This section provides a detailed description of the experimental setup, dataset preparation, evaluation metrics, and baseline comparisons used to validate the effectiveness of PVAL for detecting localizing, and quantifying solar panels in satellite imagery.

4.1. Experiment Preparation

To rigorously assess the PVAL framework, we conducted experiments in two computational environments: The first environment utilized OpenAI’s platform for fine-tuning the GPT-4o-2024-08-06 model, allowing direct access to the service’s proprietary architecture and pre-trained capabilities. In parallel, we employed a high-performance computing server equipped with NVIDIA A100-SXM4-80GB GPUs to train and evaluate baseline models and perform additional analyses.

Our dataset comprises more than 100,000 satellite images of residential rooftops, each meticulously annotated to indicate the presence of solar panels.

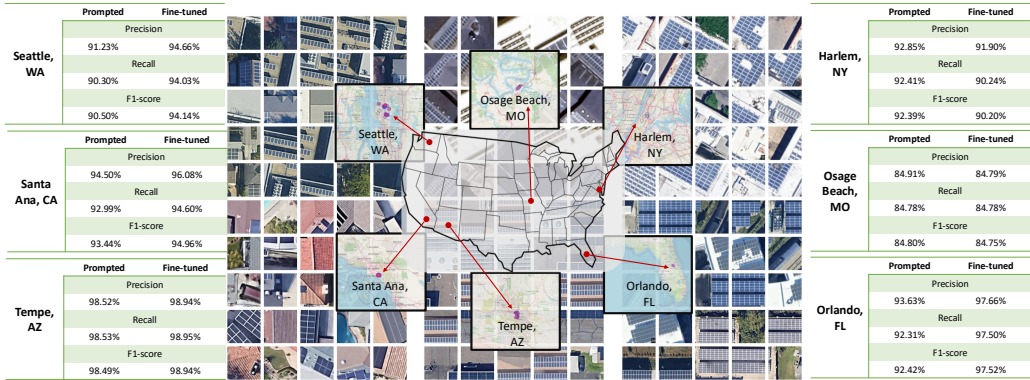


Figure 3: Sample data from six regions across the United States, with tables displaying the weighted average precision, recall, and F1-score for each region.

For a subset of the test samples, we also provided detailed spatial labels and estimated panel counts. All annotations were produced through a human-in-the-loop process, ensuring a reliable ground truth for both fine-tuning and validation. Figure 3 presents random samples from various regions.

An important consideration for PVAL was the output modality of the GPT-4o. Although GPT-4o can effectively process imagery, it produces textual descriptions rather than pixel-level segmentation masks or object-coordinate predictions. To utilize the labels, we formulated our annotations and prompts (e.g., Section 3.3.2) in a discrete, text-based manner, ensuring that the model’s outputs could be directly compared to human-generated ground truth labels. The textual output format aligns well with LLM-based workflows, providing interpretable results that can be readily integrated into downstream applications, such as powergrid operation tools and decision support systems.

4.2. Benchmark Models and Evaluation Metrics

To compare the proposed PVAL against established methods, we evaluated a range of benchmark models spanning traditional machine learning techniques, convolutional neural networks (CNNs), and transformer-based architectures. Traditional ML approaches such as SVM, Decision Trees, Random Forest, and Logistic Regression utilized Histogram of Oriented Gradients (HOG) features. For CNN-based baselines, we fine-tuned U-Net [11], ResNet-152 [34], VGG-19 [35], and Inception-v3 [36], adapting their output layers for binary classification. These models leverage deep feature hierarchies for ro-

bust representation learning. We also evaluated a Vision Transformer (ViT-Base-16 [37]), which is pre-trained on ImageNet-21k and processes images as patches through transformer layers. Together, these baseline methods provide a comprehensive reference point for assessing the effectiveness of our proposed LLM-based approach.

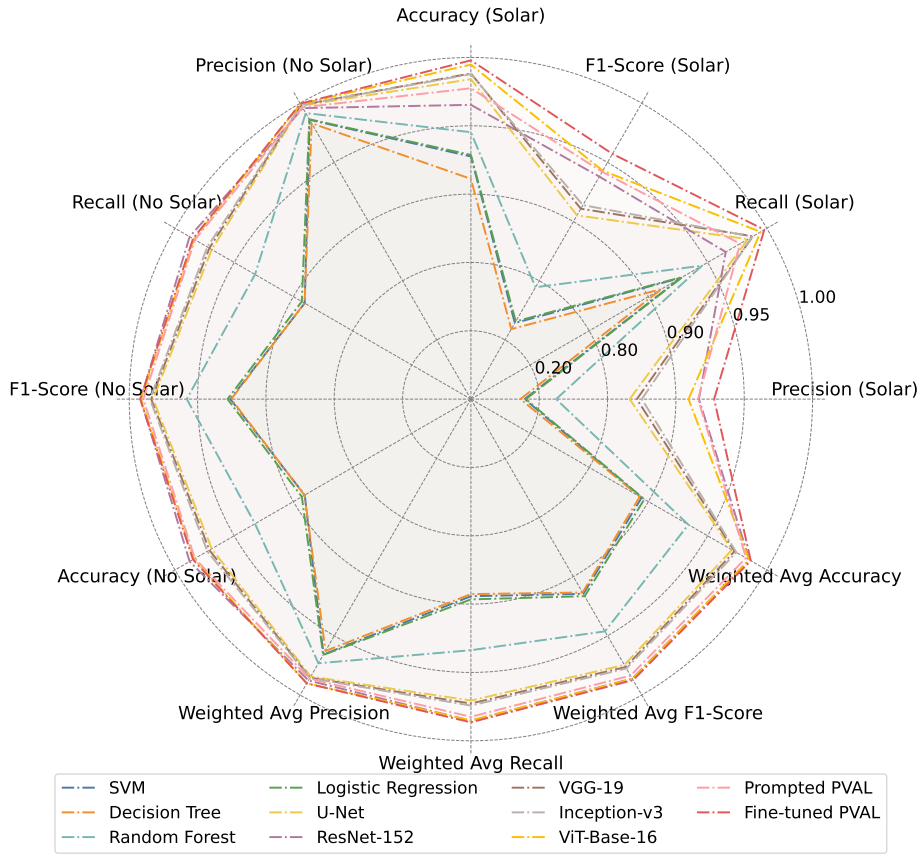


Figure 4: Radar chart comparing the performance of various models on solar panel detection. Metrics include precision, recall, F1-score, and accuracy for "No Solar," "Solar," and weighted averages. "Prompted PVAL" and "Fine-tuned PVAL" are highlighted in orange and red, respectively, to emphasize their performance.

To comprehensively assess the performance of the proposed method and other benchmarks, we employed the following evaluation metrics:

Precision: The ratio of true positive detections (TP) to the total number

Table 1: PVAL Prompt vs PVAL Fine-tuned for Solar Panel Detection Across Regions

Methods	Region	Solar				No Solar				Weighted Average			
		Precision	Recall	F1-Score	Accuracy	Precision	Recall	F1-Score	Accuracy	Precision	Recall	F1-Score	Accuracy
PVAL Prompt	Santa Ana, CA	66.48%	90.98%	76.82%	90.98%	98.60%	93.29%	95.87%	93.29%	94.50%	92.99%	93.44%	92.99%
	Seattle, WA	78.72%	92.50%	85.06%	92.50%	96.55%	89.36%	92.82%	89.36%	91.23%	90.30%	90.50%	90.30%
	Tempe, AZ	98.63%	99.77%	99.20%	99.77%	96.55%	86.05%	91.36%	86.05%	98.52%	98.53%	98.49%	98.53%
	Orlando, FL	82.86%	100.00%	90.62%	100.00%	100.00%	87.76%	93.48%	87.76%	93.63%	92.31%	92.42%	92.31%
	Osage Beach, MO	81.82%	85.71%	83.72%	85.71%	87.50%	84.00%	85.71%	84.00%	84.91%	84.78%	84.80%	84.78%
	Harlem, NY	88.37%	97.44%	92.68%	97.44%	97.22%	87.50%	92.11%	87.50%	92.85%	92.41%	92.39%	92.41%
PVAL Fine-tuned	Santa Ana, CA	71.18%	99.15%	82.87%	99.15%	99.86%	93.91%	96.79%	93.91%	96.08%	94.60%	94.96%	94.60%
	Seattle, WA	84.78%	97.50%	90.70%	97.50%	98.86%	92.55%	95.60%	92.55%	94.66%	94.03%	94.14%	94.03%
	Tempe, AZ	99.08%	99.77%	99.42%	99.77%	97.62%	91.11%	94.25%	91.11%	98.94%	98.95%	98.94%	98.95%
	Orlando, FL	93.55%	100.00%	96.67%	100.00%	100.00%	96.08%	98.00%	96.08%	97.66%	97.50%	97.52%	97.50%
	Osage Beach, MO	85.00%	80.95%	82.93%	80.95%	84.62%	88.00%	86.27%	88.00%	84.79%	84.78%	84.75%	84.78%
	Harlem, NY	82.98%	100.00%	90.70%	100.00%	100.00%	81.40%	89.74%	81.40%	91.90%	90.24%	90.20%	90.24%

of positive detections ($TP + FP$), measuring the accuracy of the model’s positive predictions. It is defined as:

$$\text{Precision} = \frac{TP}{TP + FP} \tag{5}$$

Recall: The ratio of true positive detections (TP) to the total number of actual positives ($TP + FN$), reflecting the model’s ability to identify all instances of solar panels. It is defined as:

$$\text{Recall} = \frac{TP}{TP + FN} \tag{6}$$

F1 Score: The harmonic mean of precision and recall, providing a balanced measure of the model’s overall performance. F1-Score is defined as:

$$\text{F1 Score} = 2 \cdot \frac{\text{Precision} \cdot \text{Recall}}{\text{Precision} + \text{Recall}} \tag{7}$$

Accuracy of Location and Quantity: Since the model generates location or quantity descriptions (e.g., “left”, “top-left”, or “10 to inf”), the accuracy metric is defined as the percentage of descriptions that are **exactly correct**, calculated using the formula:

$$\text{Accuracy} = \frac{\text{Number of Correct Descriptions}}{\text{Total Number of Descriptions}} \tag{8}$$

4.3. Result Analysis for Prompting Strategies

The first part of Table 1 presents the performance of PVAL with prompt strategies for solar panel detection across various regions. The class “Solar”

indicates images containing solar panels, while the class “No Solar” indicates images without solar panels.

Notably, existing open-source models, such as Vision Transformer (ViT), Inception-v3, and other large pre-trained architectures, face significant challenges when applied to domain-specific tasks like solar panel detection. For example, ViT-Base-16, pre-trained on ImageNet-21k, is optimized for general object recognition and lacks exposure to domain-specific objects such as solar panels. As a result, these models fail to produce meaningful results in solar panel detection tasks without extensive fine-tuning and domain adaptation, which require considerable computational resources and specialized datasets. This limitation renders them impractical for organizations or researchers with limited access to these resources.

Unlike the traditional pre-trained vision model, the PVAL can adapt to solar panel detection directly by leveraging contextual understanding and task-specific prompts.

We use a green background to mark the values where prompted PVAL can achieve the same or better performance compared to the fine-tuned PVAL. Notably, prompted PVAL achieves competitive average accuracy and F1-scores in regions such as Osage Beach, MO, and Harlem, NY, without requiring fine-tuning or additional training. A concise comparison can be seen in Figure 3. These findings underscore its potential as a cost-effective and efficient solution for organizations seeking robust performance in solar panel detection without incurring the high costs associated with data collection, annotation, and model fine-tuning.

4.4. Result Analysis for Fine-tuned Models

Table 2: Comprehensive Results Table for Solar Panel Detection Methods after fine-tuning or training

	Methods	Solar				No Solar				Weighted Average			
		Precision	Recall	F1-Score	Accuracy	Precision	Recall	F1-Score	Accuracy	Precision	Recall	F1-Score	Accuracy
Small Size Models	SVM	15.70%	71.01%	25.72%	71.01%	94.40%	56.16%	70.42%	56.16%	86.28%	57.69%	65.81%	57.69%
	Decision Tree	14.48%	64.46%	23.65%	64.46%	93.22%	56.22%	70.14%	56.22%	85.10%	57.07%	65.35%	57.07%
	Random Forest	24.94%	78.12%	37.81%	78.12%	96.67%	72.96%	83.15%	72.96%	89.27%	73.49%	78.48%	73.49%
	Logistic Regression	16.09%	71.48%	26.27%	71.48%	94.57%	57.14%	71.24%	57.14%	86.48%	58.62%	66.60%	58.62%
Large Size Models	U-Net [11]	46.47%	93.64%	62.11%	93.64%	99.17%	87.59%	93.02%	87.59%	93.74%	88.22%	89.83%	88.22%
	ResNet-152 [34]	66.74%	86.13%	75.20%	86.13%	98.35%	95.06%	96.68%	95.06%	95.09%	94.14%	94.46%	94.14%
	VGG-19 [35]	48.56%	95.32%	64.35%	95.32%	99.40%	88.39%	93.57%	88.39%	94.15%	89.10%	90.55%	89.10%
	Inception-v3 [36]	50.03%	95.11%	65.57%	95.11%	99.37%	89.08%	93.94%	89.08%	94.28%	89.70%	91.02%	89.70%
	ViT-Base-16 [37]	63.71%	97.91%	77.19%	97.91%	99.74%	93.59%	96.57%	93.59%	96.03%	94.03%	94.57%	94.03%
	PVAL Fine-tuned	71.18%	99.15%	82.87%	99.15%	99.86%	93.91%	96.79%	93.91%	96.08%	94.60%	94.96%	94.60%

The fine-tuned PVAL demonstrates superior performance compared to the prompted PVAL across most metrics and geographical regions, as shown

in Table 1. The fine-tuned model achieves the highest accuracy in five out of six regions studied. Fine-tuning significantly improves precision, recall, and F1-scores for solar panel detection across multiple regions, including Santa Ana (CA), Seattle (WA), Tempe (AZ), and Orlando (FL). For instance, the fine-tuned model achieved a F1-score of 97.52% in Orlando, compared to 92.42% by the prompted approach, representing a clear advantage.

The fine-tuned PVAL not only surpasses the prompted counterpart but also outperforms traditional benchmark models. We take Santa Ana as an example, as shown in Table 2, highlighting the impact of domain adaptation on the specialized task of solar panel detection.

The fine-tuned PVAL model achieves remarkable results, including a solar F1-score of 82.87% and a weighted average F1-score of 94.96%. Additionally, it attains an impressive solar recall of 99.15%, demonstrating its ability to detect solar panels with near-perfect completeness. These metrics make fine-tuned PVAL the best-performing model, showcasing the effectiveness of leveraging a fine-tuned LLM for solar panel detection tasks.

However, benchmark models such as ResNet-152 and ViT-Base-16 also provide valuable insights into the challenges and trade-offs inherent in solar panel detection. ResNet-152 achieves the highest recall (95.06%) and accuracy (95.06%) for the “No Solar” class among all models. This indicates that ResNet-152 is highly effective at minimizing false negatives for predictions of image without solar panels. The reason for this lies in its deep architecture and hierarchical feature extraction, which enable it to capture subtle differences between solar and non-solar regions. However, its relatively lower performance in the solar category (F1-score of 75.20%) suggests that the model struggles with balancing class-specific trade-offs, likely due to the lack of task-specific knowledge.

ViT-Base-16 also exhibits strong performance, achieving a F1-score of 77.19% for the “solar” class and a weighted average F1-score of 94.57%. Its ability to handle both “Solar” and “No Solar” classes effectively highlights the strength of transformer-based architectures in modeling long-range dependencies and capturing complex spatial features. Nonetheless, ViT-Base-16’s performance, while competitive, is slightly inferior to Fine-tuned PVAL, primarily due to the lack of domain-specific adaptation. The reliance on general-purpose features hinders its ability to achieve optimal results in a specialized task like solar panel detection.

Figure 4 highlights the performance of a fine-tuned PVAL, which combines PV-specific training with the flexibility of generative transformers.

Fine-tuning on solar panel data enables high recall and precision across all categories, outperforming all baseline models in achieving this balance.

4.5. Scalability and adaptability of PVAL

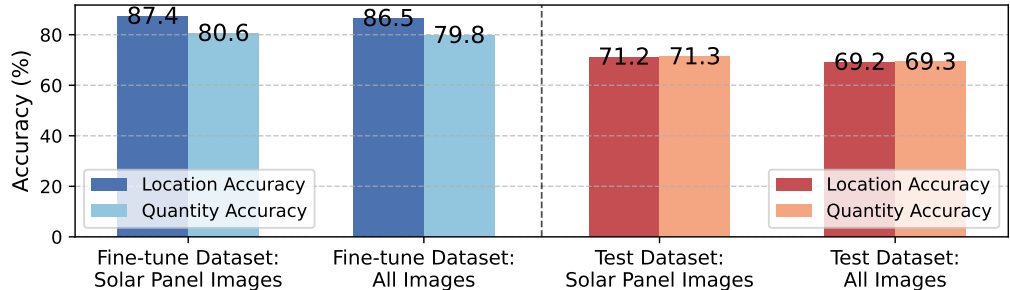


Figure 5: Accuracy of solar panel location and quantity for fine-tune and test datasets.

In addition to its scalability to multiple regions, as shown in Sections 4.3 and 4.4, we demonstrate PVAL also exhibits adaptability to diverse tasks, including localization and quantification for solar panels.

Figure 5 highlights the prediction accuracy of the fine-tuned PVAL in identifying both the position and quantity of solar panels. The fine-tuned dataset achieves notably high accuracy, with position prediction at 87.38% for solar panel images and 86.50% across all images, reflecting the effectiveness of the model after optimization. Meanwhile, the test dataset maintains reasonable performance, with 71.24% accuracy for position prediction on solar panel images, underscoring the model’s generalizability to unseen data.

It is worth noting that the evaluation metrics for location and quantity rely on an “exact match” criterion (see Section 4.2). However, in practical applications, strict accuracy in the “location” and “quantity” metrics may not always be necessary. For instance, identifying a solar panel’s location as “left” can be acceptable for a ground truth labeled as “top-left”.

To further illustrate this, Figure 6 provides visual examples of predicted solar panel locations and quantities. The results demonstrate that PVAL effectively identified and described the positions of solar panels using descriptors such as “bottom-right”, “top-left”, and “center”, etc. These predictions closely align with manually annotated ground-truth regions. Moreover, the examples highlight the model’s robust spatial reasoning capabilities, even in



Figure 6: Examples of inferences by fine-tuned PVAL for detecting, localizing, and quantifying solar panels. The results demonstrate the model’s precision in identifying and describing the spatial positioning of solar panels in satellite imagery.

complex scenarios where solar panels are distributed across varied spatial orientations, including edges, corners, or central areas. This capacity for precise spatial interpretation underscores the model’s potential for large-scale solar panel detection tasks.

4.6. Confidence-Driven Auto-Labeling Mechanism

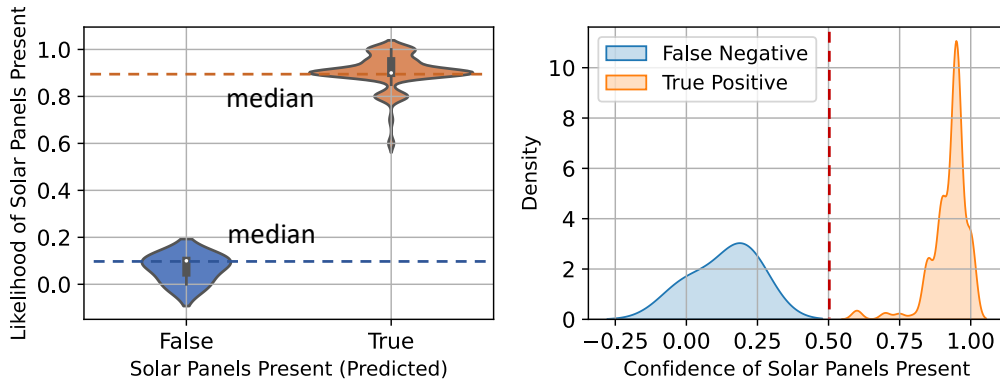


Figure 7: (Left) Violin plot showing the likelihood of solar panels present as predicted for True (“Solar”) and False (“No Solar”) classifications, along with their respective median values. (Right) Density plot of prediction confidence for True Positive and False Negative cases, generated using Kernel Density Estimation (KDE), with a vertical red line marking the threshold at 0.5.

The dual-metric approach of likelihood and confidence offers a comprehensive framework for understanding the model’s decision-making process and assessing its reliability in classifying solar panel presence. In this experiment, *likelihood* quantifies the probability of solar panel presence in an image, while *confidence* reflects the model’s internal certainty regarding its classification.

Figure 7 illustrates these metrics from two perspectives. The violin plot on the left visualizes the likelihood distributions for images classified as True (“Solar”) and False (“No Solar”). As expected, images correctly classified as True exhibit significantly higher median likelihood values than those labeled False, reaffirming the alignment between likelihood scores and the true presence of solar panels.

The density plot on the right focuses on confidence values for True Positive and False Negative outcomes. True Positive cases cluster tightly around confidence values near 1.0, demonstrating the model’s strong assurance when

making accurate predictions. Conversely, False Negatives are more prevalent at lower confidence levels, often below a 0.5 threshold indicated by the vertical red line. This trend highlights challenging scenarios where the model underestimates the likelihood of solar panels, leading to missed detections.

The density plot on the right focuses on confidence values for True Positive and False Negative outcomes. True Positive cases cluster tightly around confidence values near 1.0, demonstrating the model’s strong assurance when making accurate predictions. Conversely, False Negatives are more prevalent at lower confidence levels, often below a 0.5 threshold indicated by the vertical red line. This trend highlights challenging scenarios where the model underestimates the likelihood of solar panels, leading to missed detections.

By analyzing likelihood and confidence together, this experiment underscores their complementary roles in improving the auto-labeling mechanism. High-likelihood, high-confidence predictions correspond to reliable classifications, suitable for automated labeling with minimal manual intervention. To enhance system performance, decision thresholds can be adjusted to balance sensitivity and precision, thereby reducing False Negatives without compromising the model’s overall reliability. This adaptive mechanism not only ensures accurate auto-labeling but also facilitates targeted interventions, streamlining the management of extensive solar panel datasets for downstream tasks.

5. Conclusion

This paper investigates how LLMs, guided by data engineering, prompt engineering, and fine-tuning, can efficiently detect solar panels in satellite imagery, reducing reliance on extensive labeled datasets and computational resources. The proposed PVAL framework surpasses existing methods with superior scalability across diverse environments and adaptability to multiple tasks. Additionally, by incorporating likelihood and confidence metrics, it enhances interpretability and provides valuable decision-making support for grid operators. These results demonstrate the potential of LLMs as cost-effective tools to accelerate renewable energy integration and enhance the resilience of microgrids and active ADNs.

Acknowledgments

The author expresses sincere gratitude to Yizheng Liao for his insightful suggestions regarding the utilization of prompt engineering and fine-tuning.

We also acknowledge meaningful suggestions from Dr. Erik Blasch.

References

- [1] C. Xiao, Y. Liao, Y. Weng, Distribution grid line outage identification with unknown pattern and performance guarantee, *IEEE Transactions on Power Systems* (2023).
- [2] J. Yuan, Y. Weng, C.-W. Tan, Determining maximum hosting capacity for pv systems in distribution grids, *International Journal of Electrical Power & Energy Systems* 135 (2022) 107342.
- [3] M. Guo, Q. Cui, Y. Weng, Graph mining for classifying and localizing solar panels in distribution grids, in: *2023 Panda Forum on Power and Energy (PandaFPE)*, IEEE, 2023, pp. 1743–1747.
- [4] K. Abdulmawjood, S. S. Refaat, W. G. Morsi, Detection and prediction of faults in photovoltaic arrays: A review, in: *2018 IEEE 12th International Conference on Compatibility, Power Electronics and Power Engineering (CPE-POWERENG 2018)*, IEEE, 2018, pp. 1–8.
- [5] J. M. Malof, K. Bradbury, L. M. Collins, R. G. Newell, A. Serrano, H. Wu, S. Keene, Image features for pixel-wise detection of solar photovoltaic arrays in aerial imagery using a random forest classifier, in: *2016 IEEE International Conference on Renewable Energy Research and Applications (ICRERA)*, IEEE, 2016, pp. 799–803.
- [6] J. Yuan, Y. Weng, Support matrix regression for learning power flow in distribution grid with unobservability, *IEEE Transactions on Power Systems* 37 (2) (2021) 1151–1161.
- [7] J. Wu, J. Yuan, Y. Weng, R. Ayyanar, Spatial-temporal deep learning for hosting capacity analysis in distribution grids, *IEEE Transactions on Smart Grid* 14 (1) (2022) 354–364.
- [8] M. Guo, Y. Weng, L. Ye, Y. C. Lai, Continuous variational quantum algorithms for time series, in: *2023 International Joint Conference on Neural Networks (IJCNN)*, IEEE, 2023, pp. 01–08.

- [9] N. H. B. Ishak, I. S. B. Isa, M. K. B. Osman, K. B. Daud, M. Z. B. Ab Hamid, M. S. B. Jadin, Automated cnn-based semantic segmentation for thermal image of solar photovoltaic (pv) panel, in: 2024 IEEE 14th International Conference on Control System, Computing and Engineering (ICCSCE), IEEE, 2024, pp. 203–208.
- [10] J. Yu, Z. Wang, A. Majumdar, R. Rajagopal, Deepsolar: A machine learning framework to efficiently construct a solar deployment database in the united states, *Joule* 2 (12) (2018) 2605–2617.
- [11] C. Bouaziz, M. EL Koundi, G. Ennine, Integrated solar panel detection and energy production estimation using unet and high-resolution imagery, Ghaleb, Integrated Solar Panel Detection and Energy Production Estimation Using Unet and High-Resolution Imagery.
- [12] Y. Weng, Q. Cui, M. Guo, Transform waveforms into signature vectors for general-purpose incipient fault detection, *IEEE Transactions on Power Delivery* 37 (6) (2022) 4559–4569.
- [13] Q. Cui, Y. Weng, M. Guo, Sig2vec: Dictionary design for incipient faults in distribution systems, in: 2023 IEEE Power & Energy Society General Meeting (PESGM), IEEE, 2023, pp. 1–5.
- [14] S. Luo, Y. Weng, E. Cook, R. Trask, E. Blasch, Solar panel identification under limited labels, in: 2022 IEEE Power & Energy Society General Meeting (PESGM), IEEE, 2022, pp. 1–5.
- [15] J. Achiam, S. Adler, S. Agarwal, L. Ahmad, I. Akkaya, F. L. Aleman, D. Almeida, J. Altenschmidt, S. Altman, S. Anadkat, et al., Gpt-4 technical report, arXiv preprint arXiv:2303.08774 (2023).
- [16] D. Driess, F. Xia, M. S. Sajjadi, C. Lynch, A. Chowdhery, B. Ichter, A. Wahid, J. Tompson, Q. Vuong, T. Yu, et al., Palm-e: An embodied multimodal language model, arXiv preprint arXiv:2303.03378 (2023).
- [17] R. Girdhar, A. El-Nouby, Z. Liu, M. Singh, K. V. Alwala, A. Joulin, I. Misra, Imagebind: One embedding space to bind them all, in: Proceedings of the IEEE/CVF Conference on Computer Vision and Pattern Recognition, 2023, pp. 15180–15190.

- [18] M. Guo, M. Guo, J. Su, J. Chen, J. Yu, J. Wang, H. Du, P. Sahu, A. A. Sharma, F. Jin, Bayesian iterative prediction and lexical-based interpretation for disturbed chinese sentence pair matching, in: Proceedings of the ACM on Web Conference 2024, 2024, pp. 4618–4629.
- [19] M. Guo, M. Guo, E. T. Dougherty, F. Jin, Msq-biobert: Ambiguity resolution to enhance biobert medical question-answering, in: Proceedings of the ACM Web Conference 2023, 2023, pp. 4020–4028.
- [20] M. Guo, Transparent ai enhancements in human language and agent actions, Ph.D. thesis, The George Washington University (2024).
- [21] C. Xiao, Y. Liao, Y. Weng, Privacy-preserving line outage detection in distribution grids: An efficient approach with uncompromised performance, IEEE Transactions on Power Systems (2024).
- [22] N. Patel, M. Kulkarni, M. Parmar, A. Budhiraja, M. Nakamura, N. Varshney, C. Baral, Multi-logieval: Towards evaluating multi-step logical reasoning ability of large language models, arXiv preprint arXiv:2406.17169 (2024).
- [23] R. Stureborg, D. Alikaniotis, Y. Suhara, Large language models are inconsistent and biased evaluators, arXiv preprint arXiv:2405.01724 (2024).
- [24] E. Blasch, X. Li, G. Chen, W. Li, Image quality assessment for performance evaluation of image fusion, in: 2008 11th International Conference on Information Fusion, IEEE, 2008, pp. 1–6.
- [25] T. Xu, S. Wu, S. Diao, X. Liu, X. Wang, Y. Chen, J. Gao, Sayself: Teaching llms to express confidence with self-reflective rationales, arXiv preprint arXiv:2405.20974 (2024).
- [26] E. Blasch, É. Bossé, D. A. Lambert, High-level information fusion management and systems design, Artech House, 2012.
- [27] A. Vaswani, Attention is all you need, Advances in Neural Information Processing Systems (2017).
- [28] S. Josefsson, The base16, base32, and base64 data encodings, Tech. rep. (2006).

- [29] T. Khot, H. Trivedi, M. Finlayson, Y. Fu, K. Richardson, P. Clark, A. Sabharwal, Decomposed prompting: A modular approach for solving complex tasks, arXiv preprint arXiv:2210.02406 (2022).
- [30] K. Chu, Y.-P. Chen, H. Nakayama, A better llm evaluator for text generation: The impact of prompt output sequencing and optimization, arXiv preprint arXiv:2406.09972 (2024).
- [31] T. B. Brown, Language models are few-shot learners, arXiv preprint arXiv:2005.14165 (2020).
- [32] A.-L. Joussetme, J. P. de Villiers, A. De Freitas, E. Blasch, V. Dragos, G. Pavlin, P. Costa, K. B. Laskey, C. Laudy, Uncertain about chatgpt: enabling the uncertainty evaluation of large language models, in: 2023 26th International Conference on Information Fusion (FUSION), IEEE, 2023, pp. 1–8.
- [33] R. Tinn, H. Cheng, Y. Gu, N. Usuyama, X. Liu, T. Naumann, J. Gao, H. Poon, Fine-tuning large neural language models for biomedical natural language processing, Patterns 4 (4) (2023).
- [34] K. He, X. Zhang, S. Ren, J. Sun, Deep residual learning for image recognition, in: Proceedings of the IEEE conference on computer vision and pattern recognition, 2016, pp. 770–778.
- [35] K. Simonyan, Very deep convolutional networks for large-scale image recognition, arXiv preprint arXiv:1409.1556 (2014).
- [36] C. Szegedy, V. Vanhoucke, S. Ioffe, J. Shlens, Z. Wojna, Rethinking the inception architecture for computer vision, in: Proceedings of the IEEE conference on computer vision and pattern recognition, 2016, pp. 2818–2826.
- [37] A. Dosovitskiy, An image is worth 16x16 words: Transformers for image recognition at scale, arXiv preprint arXiv:2010.11929 (2020).